Available online at www.sciencedirect.com
ScienceDirect
Journal of Hydrodynamics
2017,29(6):1035-1043
DOI: 10.1016/S1001-6058(16)60817-X
www.sciencedirect.com/science/journal/l0016058

The gas jet behavior in submerged Laval nozzle flow *

Zhao-xin Gong（宫兆新）, Chuan-jing Lu（鲁传敬）, Jie Li（李杰）, Jia-yi Cao（曹嘉怡）
Department of Engineering Mechanics, MOE Key laboratory of Hydrodynamics, Shanghai Jiao Tong University, Shanghai 200240, China, E-mail: jackyff@sjtu.edu.cn

(Received September 30, 2015, Revised April 12, 2016)

Abstract: The behavior of the combustion gas jet in a Laval nozzle flow is studied by numerical simulations. The Laval nozzle is installed in an engine and the combustion gas comes out of the engine through the nozzle and then injects into the surrounding environment. First, the jet injection into the air is simulated and the results are verified by the theoretical solutions of the 1-D isentropic flow. Then the behavior of the gas jet in a submerged Laval nozzle flow is simulated for various water depths. The stability of the jet and the jet evolution with a series of expansion waves and compression waves are analyzed, as well as the mechanism of the jet in a deep water depth. Finally, the numerical results are compared with existing experimental data and it is shown that the characteristics of the water blockage and the average values of the engine thrust are in good agreement and the unfixed engine in the experiment is the cause of the differences of the frequency and the amplitude of the oscillation.

Key words: Gas jet, Laval nozzle, water blockage, shock wave

Introduction

The underwater ignition technique is adopted by many submarine-launched missiles. After the ignition, the combustion gas injects into the water with a high velocity to form a submerged gas jet. The presence of a two-phase interface with a large density difference makes the jet development much more complicated, unstable and difficult to predict. Especially under an over-expanded nozzle flow condition, shock waves appear to induce an intricate flow system. The interaction between the shock waves and the turbulent fluid around the nozzle can make the flow unsteady in the shock wave position and lead to the flow instability. Meanwhile, such uncertainties can influence the missile attitude and the missile stability. A better understanding of the relevant characteristics and the mechanisms of the submerged gas jet is imperative for optimizing the underwater engine design.

The submerged gas jets were classified into two regimes in previous studies. At low flow rates, the bubbling regime is observed, characterized by the production of bubbles that break near the orifice and rise with buoyancy or density effects[1]. At higher flow rates, the jetting regime predominates, with the gas flowing from the orifice continuously[2,3]. Basically the submerged gas jet studied here is mostly in the latter regime.

The submerged high-speed gas jets were studied using experimental and numerical methods. Mori et al.[4] defined a quantitative metric to describe the bubbling-jetting transition point and found that the transition occurred when the jet velocity at the orifice reached sonic. Loth and Faeth[5] studied the round turbulent air jets injecting into still water at various under-expanded jetting conditions. They measured the presence of a shock cell structure downstream of the orifice by using a pilot-probe device. Shi et al.[6] observed the flow field of the underwater supersonic gas jets and found that the strong flow oscillation was related to the shock wave feedback in the gas phase. Weiland and Vlachos[7] performed direct measurements of the interfacial behavior of the water-submerged gas jets with Mach numbers ranging from subsonic to supersonic ranges using high-speed digital photograph and shadowgraph. A new method was proposed to determine the jet penetration distance. It was found that the gas jet turns to be stable when the Mach number reaches 1.8. Zhou and Yu[8] experimen-

* Project supported by the National Natural Science Foundation of China (Grant No. 11572194)
Biography: Zhao-xin Gong (1982-), Female, Ph. D., Assistant Professor
Corresponding author: Jia-yi Cao,
E-mail: jycao@sjtu.edu.cn

tally studied the expansion process and interaction process of combustion-gas jets in the liquid under different injection pressures and nozzle diameters by means of a high-speed camera system and indicated that the gas-curtain is formed by the turbulent mixing process. Xue et al.[9] also adopted the high-speed digital camera system to investigate the expansion processes of the Taylor cavities formed by combustion-gas jets and the mixing characteristics of gasliquid and discussed the relevant influence factors on jet expansions. Roumbas et al.[10] investigated the scalar transport in the near field of two square coaxial air jet flow and analyzed the flow structures by using different sensors to record the velocity and temperature information. It is worth noting that the experimental technique of PIV can be applied to study the jets flow with lower Reynolds numbers, but are still unable to deal with high-speed jets problems[11,12].

Besides these experimental studies, some numerical simulations also carried out. Loth and Faeth[5] used an on-fluid model and a locally-homogeneous-flow approximation to treat the multiphase effects. They applied the adapted jet exit conditions to handle the complicated gas flows. In the numerical research of the multiphase flow field of the underwater launch, Lu et al.[13] set up a two-fluid model to calculate the multiphase flow. They assumed that the water flow was potential and the gas flow was quasi-1D and inviscid. An isobaric bubble model was adopted to simplify the jet flow ejected into water through a nozzle and the time-stepping algorithm was used to calculate the gas-water flow coupled with the missile's motion. On the basis of Lu's work, Zhong et al.[14] improved the bubble model and introduced the compressible Navier-Stokes equations to simulate the coupled flow. He et al.[15] employed the Level Set method to identify the interface between the gas jet and the surrounding water. Gan et al.[16] adopted a mixture model and the Navier-Stocks equation to simulate the multiphase flow field of the underwater ignition. Cheng and Liu[17] developed a coupling algorithm for water flows and gas flow in exhausted gas bubble of missile launched underwater and described the bubble evolution in detail. Vuorinen et al.[18] carried out LES to study the effect of nozzle pressure ratios on the characteristics of highly underexpanded jets and visualized the transient stages and revealed the shock speeds and duration of the transient stages. Schmitt et al.[19] investigated the supersonic methane injection in an engine and exhibtied the flow field evolution, mixture formation and combustion process in detail. Ghaseml et al.[20] used LES to investigate the compressible subsonic turbulent jets starting from a smooth contraction nozzle and visualize the evolution of the vertical structures. Instead of gas jet, Peng et al.[21] numerically studied high-speed submerged water jet issuing from a sheathed shard-edge orifice nozzle and observed the periodically shedding of cavitation clouds.

1. Numerical simulation methodology

1.1 *Problem statement*

In this paper, the gas jet behaviors in the underwater Laval nozzle flow are numerically studied. In view of the fact that the jet experiment in a pressure water tank is usually conducted under a high Froude number condition and with a short duration of ignition, the gravity effect can be neglected and an axisymmetric model is used to simulate the flow field. The entire test facility consists of the nozzle, the engine and the pressure water tank. The combustion gas comes out of the engine through a Laval nozzle and then injects into the surrounding environment. At first, a board is placed in the divergent section to isolate the inside gas from the outside water. When the pressure difference between the gas and the water reaches a certain value, the board is removed. The Laval nozzle is established horizontally inside a fixed engine. The computational domain is shown in Fig.1.

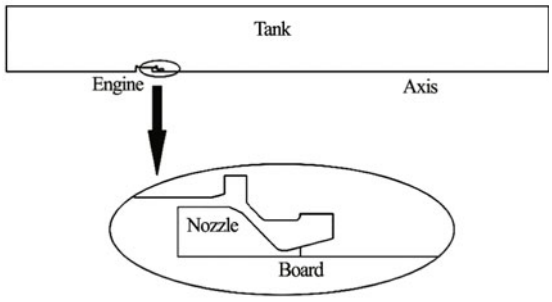

Fig.1 Diagram of the computational domain

1.2 *Governing equations*

The combustion gas jet injection is a complex transient multiphase process. It involves a complicated interaction between the combustion gas and the surrounding enviroment. The mixture model is adopted to solve the two phase flow field and the volume fraction is used to describe the distribution of the combustion gas and the ambient media(air/water). The RNG k-ε turbulent model is taken to simulate the turbulence effect.

The compressible Navier-Stokes equations can be written as:

$$\frac{\partial \rho}{\partial t}+\frac{\partial}{\partial x_i}(\rho u_i)=0 \tag{1}$$

$$\frac{\partial}{\partial t}(\rho u_i)+\frac{\partial}{\partial x_j}(\rho u_j u_i)=-\frac{\partial p}{\partial x_i}+\frac{\partial}{\partial x_j}\left[\mu\left(\frac{\partial u_j}{\partial x_i}+\frac{\partial u_i}{\partial x_j}\right)\right]+F_i \tag{2}$$

$$\frac{\partial}{\partial t}\sum_{k=g,l}(\alpha_k\rho_k E_k)+\frac{\partial}{\partial x_j}\sum_{k=g,l}[\alpha_k u_{kj}(\rho_k E_k+p)]=$$

$$\frac{\partial}{\partial x_j}\left(K_{eff}\frac{\partial T}{\partial x_j}\right)+S_E \tag{3}$$

where ρ and μ are the density and the viscosity of the mixture, F_i is the body force, g and l represent the gas and the ambient media, respectively. K_{eff} is the effective conductivity $(K+K_t)$, where K_t is the turbulent thermal conductivity, defined according to the turbulence model being used. The first term on the right-hand side of the energy Eq.(3) represents the energy transfer due to the conduction. S_E includes any other volumetric heat sources. The density and the viscosity of the mixture are defined as:

$$\rho=\alpha_g\rho_g+\alpha_l\rho_l \tag{4}$$

$$\mu=\alpha_g\mu_g+\alpha_l\mu_l \tag{5}$$

where α is the volume fraction of the phase, and satisfies $\alpha_g+\alpha_l=1$.

The state equations for the gas and the ambient media and the volume fraction equation are as follows:

$$\rho_k=\frac{p}{RT},\quad k=g \tag{6a}$$

$$\rho_k=\rho_l,\quad k=l \tag{6b}$$

where the liquid density ρ_l is assumed being constant.

$$\frac{\partial}{\partial t}(\alpha_g\rho_g)+\frac{\partial}{\partial x_i}(\alpha_g\rho_g u_i)=0 \tag{7}$$

The RNG k-ε model is used to describe the turbulent flow, which contains the turbulent kinetic equationand dissipation rate equation:

$$\frac{\partial}{\partial t}(\rho k)+\frac{\partial}{\partial x_i}(\rho k u_i)=\frac{\partial}{\partial x_j}\left[\left(\mu+\frac{\mu_t}{\sigma_k}\right)\frac{\partial k}{\partial x_j}\right]+G_k+$$

$$G_b-\rho\varepsilon-Y_M \tag{8}$$

$$\frac{\partial}{\partial t}(\rho\varepsilon)+\frac{\partial}{\partial x_i}(\rho\varepsilon u_i)=\frac{\partial}{\partial x_j}\left[\left(\mu+\frac{\mu_t}{\sigma_\varepsilon}\right)\frac{\partial\varepsilon}{\partial x_j}\right]+$$

$$C_{1\varepsilon}\frac{\varepsilon}{k}(G_k+C_{3\varepsilon}G_b)-C_{2\varepsilon}\rho\frac{\varepsilon^2}{k} \tag{9}$$

where G_k and G_b represent the generations of the turbulence kinetic energy due to the mean velocity gradients and the buoyancy, respectively. Y_M represents the contribution of the fluctuating dilatation in the compressible turbulence to the overall dissipation rate. $C_{1\varepsilon}$, $C_{2\varepsilon}$ and $C_{3\varepsilon}$ are constants. σ_k and σ_ε are the turbulent Prandtl numbers for k and ε, respectively. The turbulent viscosity μ_t is computed by combining k and ε as follows

$$\mu_t=\rho C_\mu\frac{k^2}{\varepsilon} \tag{10}$$

1.3 *Boundary conditions*

Assume that the gas inside the nozzle is quiescent with $P=1\,\text{atm}$ and $T=300\,\text{K}$ at the outset. The Laval nozzle is put in 10 m, 20 m and 30 m water depth, respectively. The expansion ratio of the divergent section is 9.

The surfaces of the engine and the nozzle are set as the wall and mathematically defined as follows:

$$\boldsymbol{u}_f=\boldsymbol{u}_w,\ T_f=T_w,\ -k\left(\frac{\partial T}{\partial n}\right)_f=q_w \tag{11}$$

where the subscripts f and w represent the fluid and the wall, respectively.

The evolution of the combustion gas in the combustor is obtained from experiment[16]. Therefore, the input for the nozzle inlet is:

$$p=p(t),\ T=T(t),\ \alpha_l=0 \tag{12}$$

where $p(t)$ and $T=T(t)$ are the total pressure and the total temperature of the combustor, which are shown in Fig.2

The boundary condition for the water field is described as

$$p=p_{\text{atm}}+\rho_l gh \tag{13}$$

where p_{atm} is the atmosphere pressure, g is the acceleration of gravity, and h is the water depth.

1.4 *Numerical methods*

The finite volume method is adopted to solve the governing equations. The coupling of the velocity and

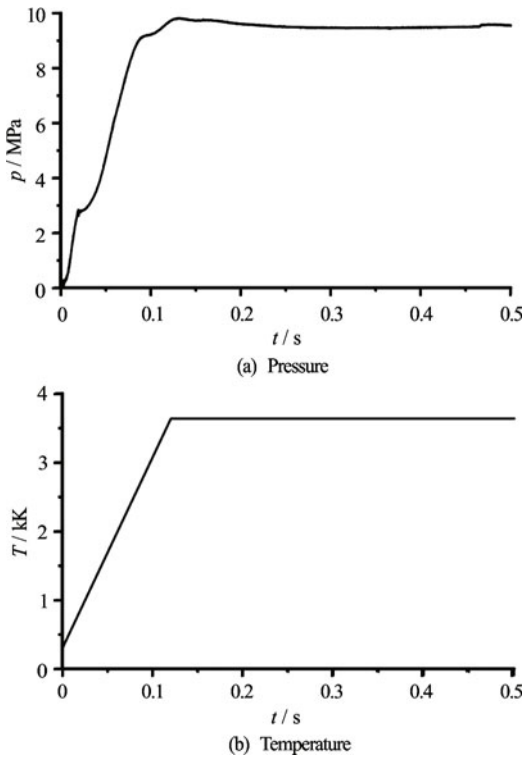

Fig.2 Boundary conditions for the nozzle inlet

pressure terms in the momentum equation is resolved by the well-known SIMPLE algorithm**.** The second upwind scheme is chosen for the equations of the momentum, the energy, the turbulent kinetic energy and the dissipation energy. The QUICK scheme is used to discretize the volume fraction. All numerical simulations are implemented by the CFD commercial solver FLUENT.

2. Results and discussions

2.1 *Validation of the numerical method*

The gas jet injection into the air is simulated in this section. Since the 1-D mathematical equations for such problem are well solved and have theoretical solutions, the numerical results are then compared with these theoretical solutions to validate the numerical method. The board in the divergent section is removed when the pressure difference between its two sides reaches 2.8 MPa. The Mach number distribution of the entire flow field is shown in Fig.3. For a better visualization of the axisymmetric issue, the contour lines of the upper part are presented in the lower part. At first, the ambient backpressure is small, the combustion jet is under an under-expanded condition and the supersonic combustion gas generates a series of expansion waves. The jet velocity increases and the pressure decreases in the expansion stage. Then, when the value of the gas pressure becomes lower than the ambient pressure, the jet starts to compress and to form a series of compression waves. The jet velocity decreases and the pressure increases in the compression stage. The jet generates an oblique shock wave in the vicinity of the strong compression wave region. As the jet pressure keeps increasing and becomes higher than the ambient pressure once again, the expansion waves re-form and then the compression waves. Due to the gas viscosity, the energy exchange between the gas jet and the surrounding air consumes the jet energy. Along the centerline direction, the jet diffusion region enlarges and the jet core region reduces, the jet velocity decreases and the expansion and compression wave structures get weakened.

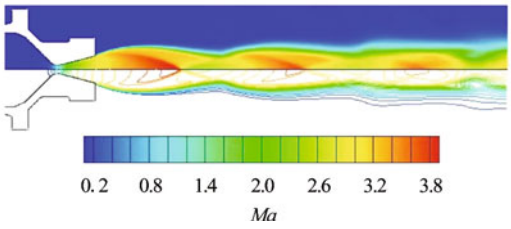

Fig.3 (Color online) Mach number distribution

In the theoretical model, the flow inside the nozzle is assumed to be a steady quasi-1D isentropic flow. As long as the nozzle inlet conditions are stabilized, the jet reaches a steady state. Neglecting the viscosity of the combustion gas, according to the isentropic flow theory of the perfect gas, the 1-D equations can be written as:

$$\frac{A_e}{A_t}=\frac{\left[\left(\frac{2}{\gamma+1}\right)\left(1+\frac{\gamma-1}{2}M_e^{\,2}\right)\right]^{(\gamma+1)/[2(\gamma-1)]}}{M_e} \tag{14}$$

$$\frac{P_0}{P_e}=\left(1+\frac{\gamma-1}{2}M_e^{\,2}\right)^{\gamma/(\gamma-1)} \tag{15}$$

$$F=(\rho_e V_e^2+P_e)A_e \tag{16}$$

where F is the thrust force of the nozzle, ρ_e, P_e, V_e, A_e are the density, the pressure, the velocity and the cross section area at the nozzle exit, respectively, P_0 is the total pressure of the combustor and A_t is the nozzle throat area.

The sonic velocity and the Mach number at the nozzle exit are defined as:

$$a_e=\sqrt{\gamma\frac{P_e}{\rho_e}},\quad M_e=\frac{V_e}{a_e} \tag{17}$$

Substituting them into Eq.(16), we obtain

$$F = (\gamma M_e^2 + 1) P_e A_e \tag{18}$$

According to the geometric profile of the nozzle and the properties of the combustion gas, the calculating parameter can be determined as:

$$\frac{A_e}{A_t} = 9\,,\quad \gamma = 1.08\,,\quad P_0 = 9.5\ \text{MPa} \tag{19}$$

With the given parameters, the theoretical results can be obtained as follows:

$$M_e = 2.9\,,\quad P_e = 1.89\times10^5\ \text{Pa}\,,\quad F = 2.3\times10^3\ \text{N} \tag{20}$$

The numerical results at the center of the nozzle exit are:

$$M_e' = 2.85\,,\quad P_e' = 2.09\times10^5\ \text{Pa}\,,\quad F' = 2.26\times10^3\ \text{N} \tag{21}$$

It can be seen that the numerical and theoretical results are in good agreement. The minor differences should come from the inviscid and 1-D flow assumption in the theoretical derivation. Such results to some extent verify the reliability and the validity of the numerical simulation method.

2.2 *Submerged gas jet behaviors*

The gas jet behaviors in the submerged Laval nozzle flow are simulated. The water is still and its depth varies from 10 m, 30 m to 50 m. The board in the divergent section is removed when the pressure difference between its two sides reaches 2.8 MPa. For each water depth, the removal time is 0.018 s, 0.024 s and 0.021 s, respectively. Figures 4-6 exhibit the evolutions of the gas jet for the water depth of 10 m, 30 m and 50 m, respectively. In all cases, the development of the jets at the initial state are almost identical. Because of the inertia of the surrounding still water, the combustion gas cannot exhaust smoothly. The nozzle is temporarily blocked by the water and the pressure inside the nozzle increases rapidly, which is called the “water blockage”. Then the high pressure pushes the water to move and the combustion gas gradually bursts through the surrounding water and begins to develop downstream. During the jet development, the moment and energy exchanges between the combustion gas and the surrounding water make the jet patterns different in different water depths. In the 10 m water depth case, the jet is relatively stable. In the 30 m water depth case, the gas-water interface gets fluctuant. In the 50 m water depth case, the jet becomes very unstable and one sees jet necking and the gas near the nozzle exit starts to expand and move backward to the nozzle exit.

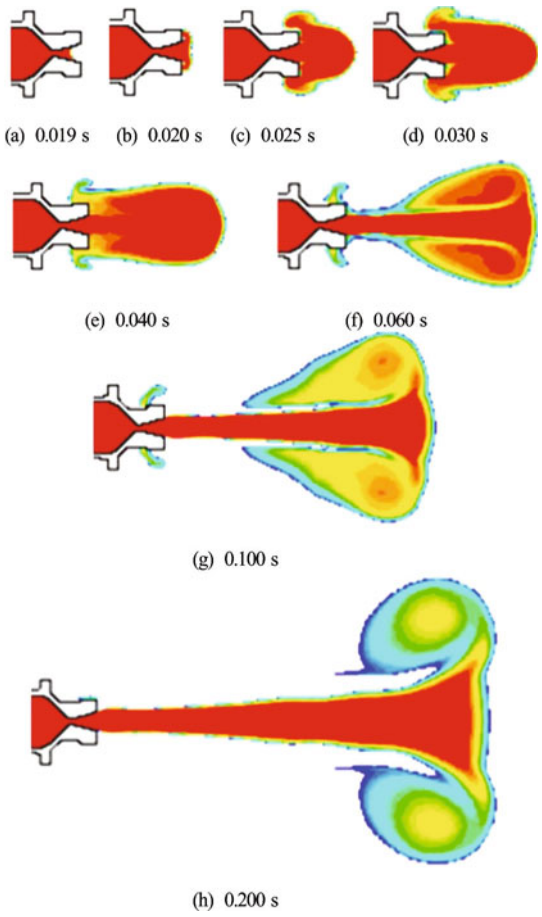

Fig.4 (Color online) Gas jet evolution in the case of 10 m water depth

Comparing the pressure variations over time among various water depths, it can be seen that the effect of the water blockage becomes stronger and the pressure leakage duration gets longer as the water depth increases, and in deeper water cases, the pressure near the nozzle exit leads to a high frequency oscillation and the instability of the jet.

Figure 7 shows the Mach number variation along the axis over time. In the 10 m water depth case, the jet near the nozzle exit is in a slightly over-expanded state, and one sees a series of expansion waves and weak compression waves. As the water depth increases to 30 m and 50 m, the jet near the nozzle is in a strongly over-expanded state and from the compression waves, shock waves are formed. The strengths of the shock waves increase with the water depth. It can be seen that the shock wave position varies with time around the nozzle exit in the 30 m and 50 m water depth cases. Therefore, the physical variables change dramatically in these areas.

Figure 8 describes the velocity vector evolution in the 50 m water depth case. The combustion gas jet

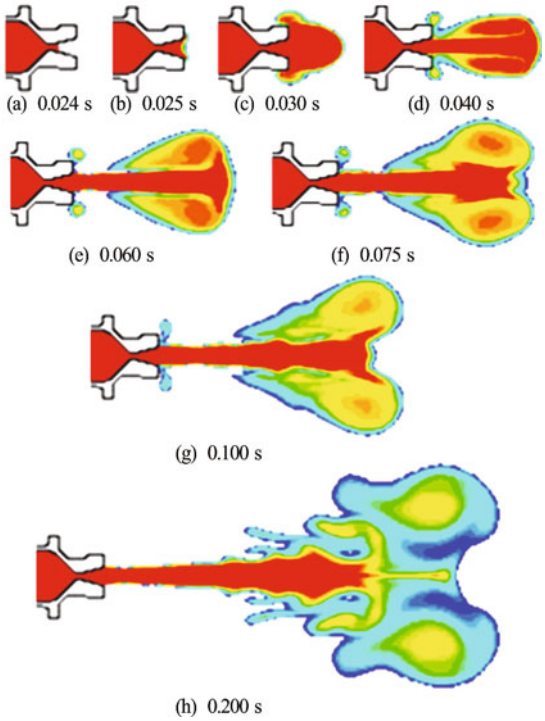

Fig.5 (Color online) Gas jet evolution in the case of 30 m water depth

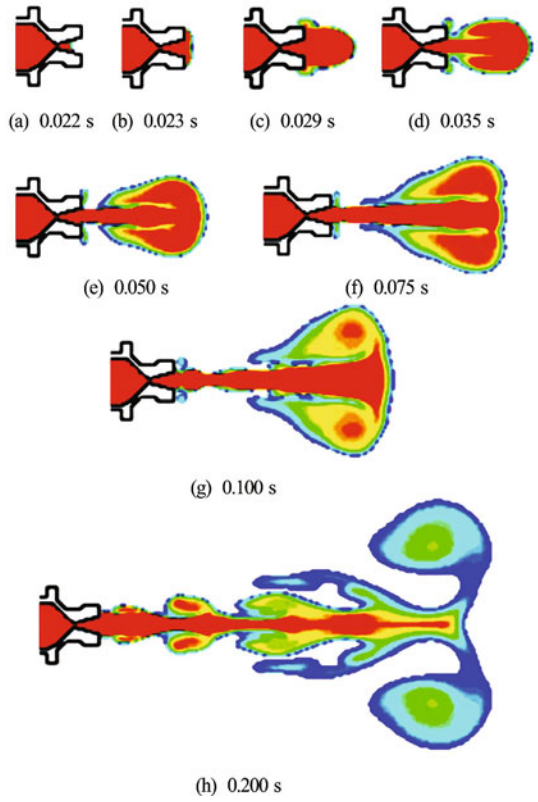

Fig.6 (Color online) Gas jet evolution in the case of 50 m water depth

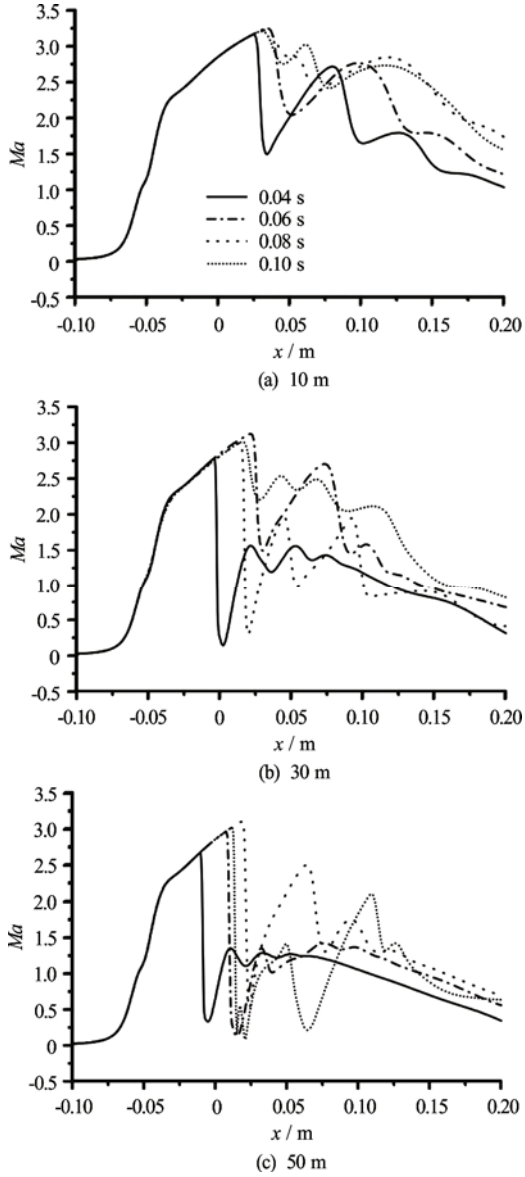

Fig.7 Mach number variations along the axis over time

sees necking, back-attack and shock wave fluctuation. In deep water depth cases, the ambient backpressure is larger than the combustion gas pressure at the nozzle exit. When the shock wave leaves the nozzle, the pressure at the first compression wave front is smaller than the ambient backpressure. In the jet mixing zone, the energy exchange between the combustion gas and the still water reduces the axial velocity of the jet outer layer rapidly. The pressure difference drives the formation of necking in the jet front, with the loss of the supersonic jet area, the decrease of the jet velocity, and the increase of the pressure and the shock wave moves backward to the nozzle. As the combustion gas keeps exhausting, the jet develops downstream. Due to the blockage of the necking, the jet also expands both

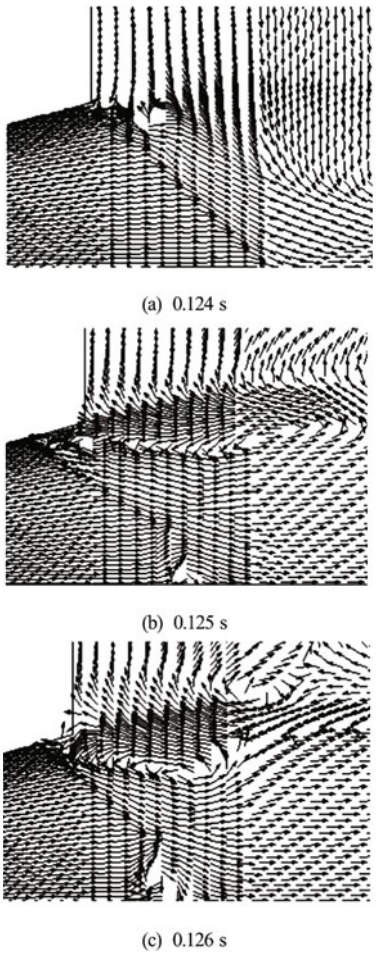

Fig.8 Velocity vector variation during the process of shock-wave moving backward in 50 m water depth

in the radial and inverted directions and strikes the nozzle bottom, which is called the back-attack. When the shock wave keeps moving backward, the necking segment goes into the expansion wave area, the jet pressure decreases and the shock wave moves downstream again. As the ambient backpressure gets higher, the necking driven force grows stronger, the extent of the jet compression becomes greater and the shock wave moves further in the backward direction. In the 50 m water depth case, the jet may shrink and break down. However, in the 30 m water depth case, because of the relatively small low pressure domain and the large axial jet velocity, the jet necking is not significant and the jet is much more stable.

Figure 9 shows the pressure variation on the axis in the shock wave front in the 30 m and 50 m water depth cases. The pressure is scaled by the ambient pressure. It can be seen that during the process of the shock wave moving backward, the pressure in the shock wave front increases and during the process of moving downstream, the pressure decreases.

Figure 10 compares the experimental and numerical results of the engine thrust in the 10 m, 30 m and 50 m water depth cases. The scaled engine experiment is carried out in a pressure water tank. The thrust includes the forces acting on both the nozzle and the engine casing. Shortly after the removal of the board, the engine is impacted by a strong instantaneous thrust from the high pressure gas because of the water blockage. Then with the jet development, the necking and the back-attack happen and the engine thrust begins to oscillate.

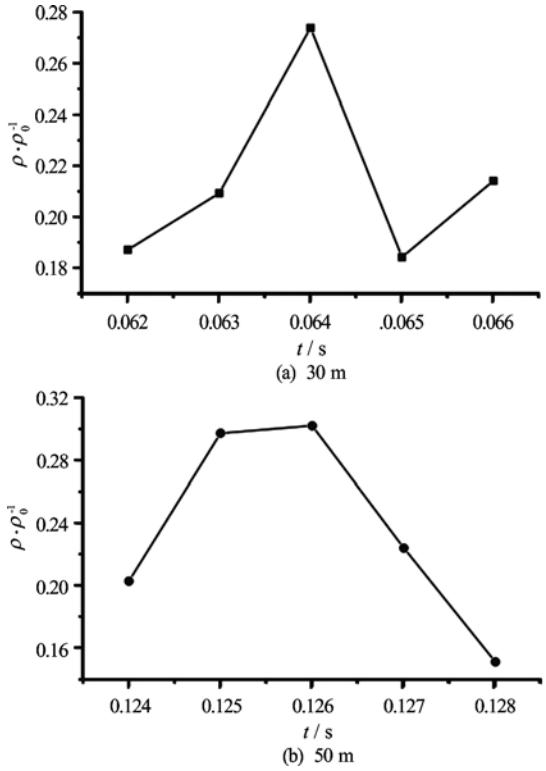

Fig.9 Pressure variation on the axis in the shock wave front

The comparison results show that the water blockage happens in both the experiment and the numerical simulation and their characteristics are consistent and the average values of the engine thrusts are in good agreement though their amplitudes and frequencies see some differences. The frequencies in the experiment are smaller. The amplitudes of the oscillations decrease as the water depth increases in the experiment. In the numerical simulation, the engine thrust becomes more unstable in deeper water depth, and with the increase of the energy generating by the shock wave oscillation, the forces acting on the engine sometimes become negative, which means that it is a pull force, which is worth noting.

In the experiment, springs are installed for the dynamometry and the engine can move in the axial direction. But in the numerical simulation, the engine is fixed. In the experiment, when the board is removed, the instantaneous thrust makes the engine move in the

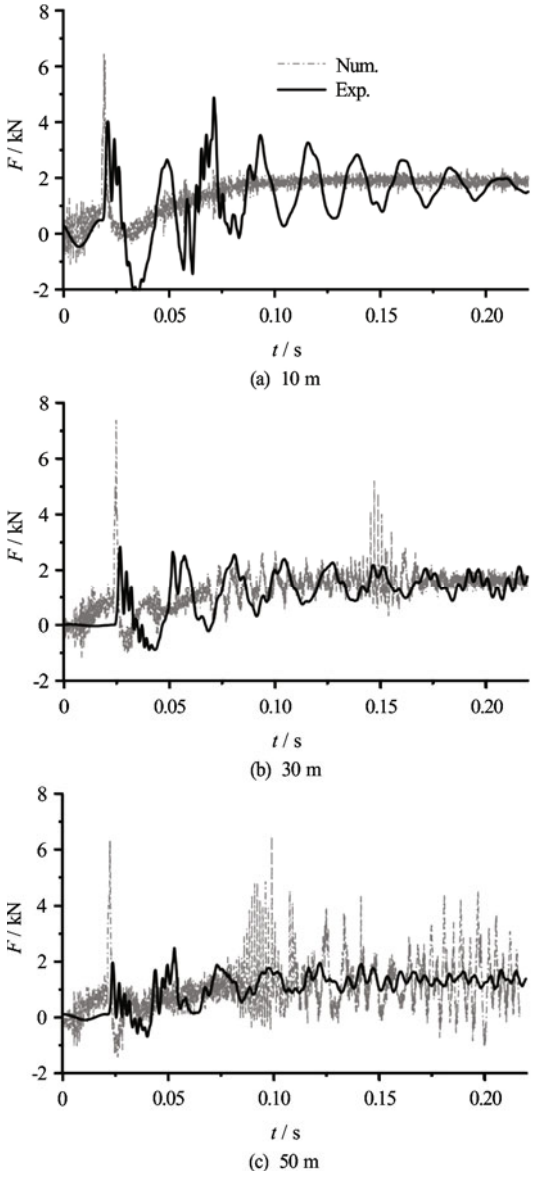

Fig.10 Comparison of the engine thrusts in experiment and numerical simulation

acting force direction and balances out some forces. Therefore, the numerical results are larger than the experimental results at the initial stage when the high pressure gas starts to exhaust.

The low frequency oscillation in the experiment may come from the inherent frequency of the test device and its dynamics response to the instantaneous thrust. The additional mass of the underwater test device causes the decay of the oscillation amplitude. In a shallower depth, the ambient pressure is smaller and the jet region is larger. Therefore, more water is driven to move and the inertia force is larger. The tested amplitude of the thrust is larger, as shown in Fig.10.

The experimental results show that a high frequency oscillation gradually appears besides the low frequency oscillation. The high frequency increases with the water depth. Such phenomena are consistent with the characteristics of the oscillation in the numerical results due to the jet instability. The unfixed engine in the experiment will affect the accuracy of the dynamometry and partly influence the jet development.

3. Conclusions

The characteristics of the submerged gas jets injected in the Laval nozzle flow are studied in this paper. The comparison between the numerical results and the theoretical solutions of the gas jet injected into the air verifies the reliability and the validity of the numerical simulation method. The submerged jet evolutions in the 10 m, 30 m and 50 m water depths are obtained, respectively.

The stability of the jet is analyzed. In the 10 m water depth, the jet near the nozzle exit is in a slightly over-expanded state and the jet is relatively stable. However, in the 30 m and 50 m water depths, the jets near the nozzle exit are in a strongly over-expanded state and the jet interfaces get fluctuant, especially in the 50 m water depth, the jet sees necking and back-attack.

The water blockage happens in both the experiment and the numerical simulation and their characteristics are consistent. Meanwhile, the average values of the engine thrusts are in good agreement though their amplitudes and frequencies see some differences because of the unfixed engine in the experiment. The engine thrust becomes more unstable in deeper water depth. It is noteworthy that the forces acting on the engine sometimes become a pull force.

References

[1] Cieslinske J. T., Mosdorf T. Gas bubble dynamics-experiment and fractal analysis [J]. *International Journal of Heat and Mass Transfer*, 2005, 48(9): 1808-1818.

[2] Weiland C. J., Vlachos P. P., Yagla J. J. Concept analysis and laboratory observations on a water piercing missile launcher [J]. *Ocean Engineering*, 2010, 37(11): 959-965.

[3] Olson B. J., Lele S. K. A mechanism for unsteady separation in over-expanded nozzle flow [J]. *Physics of Fluids*, 2013, 25(11):110809.

[4] Mori K., Ozawa Y., Sano M. Characterization of gas jet behavior at a submerged orifice in liquid metal [J]. *Transactions of the Iron and Steel Institute of Japan*, 1982, 22(5): 337-384.

[5] Loth E., Faeth G. M. Structure of underexpanded round air jets submerged in water [J]. *International Journal of Multiphase Flow*, 1989, 15(4): 589-603.

[6] Shi H. H., Wang B. Y., Dai Z. Q. Research on the mechanics of underwater supersonic gas jets [J]. *Science china Physics, Mechanics and Astronomy*, 2010, 53(3):

527-535.

[7] Weiland C. J., Vlachos P. P. Round gas jets submerged in water [J]. *International Journal of Multiphase Flow*, 2013, 48: 46-57.

[8] Zhou L., Yu Y. Experimental study on gas-curtain generation characteristics by multicombustion-gas jets in the cylindrical liquid chamber [J]. *Ocean Engineering*, 2015, 109: 410-417.

[9] Xue X., Yu Y., Zhang Q. Study on the effect of distance between the two nozzle holes on interaction of high pressure combustion-gas jets with liquid [J]. *Energy Conversion and Management*, 2014, 85: 675-686.

[10] Roumbas G., Kastrinakis E. G., Nychas S. G. Scalar transport in the near filed between two coaxial square air jets [J]. *Experimental Thermal and Fluid Science*, 2016, 78: 229-241.

[11] EI Hassan M., Meslem A. Time-resolved stereoscopic particle image velocimetry investigation of the entrainment in the near field of circular and daisy-shaped orifice jets [J]. *Physics of Fluids*, 2010, 22(3): 035107.

[12] Ghasemi A., Roussinova V., Balachandar R. et al. Reynolds number effects in the near-field of a turbulent square jet [J]. *Experimental Thermal and Fluid Science*, 2015, 61: 249-258.

[13] Lu C. J., Chen F., Fan H. et al. The fluid dynamic research on the underwater ignition of missile [J]. *Acta Aeronautica Et Astronautica Sinica*, 1992, 13(4): B124-B130.

[14] Zhong F. Q., Lu Y. X., Zhuang L. X. Numerical simulation of the complex flowfield for rocket launch under water [J]. *Journal of Astronautics*, 2000, 21(2): 1-7.

[15] He X. Y., Ma H. D., Ji C. Q. Numerical simulation of gas jets in water [J]. *Journal of Hydrodynamics, Ser. B*, 2004, 19(2): 207-212.

[16] Gan X. S., Jia Y. J., Lu C. J. et al. Research on numerical simulation of combustion gas jet under water [J]. *Journal of Solid Rocket Technology*, 2009, 32(1): 23-26.

[17] Cheng Y., Liu H. A coupling model of water flows and gas flow in exhausted gas bubble of missile launched underwater [J]. *Journal of Hydrodynamics*, *Ser. B*, 2007, 19(4): 403-411.

[18] Vuorinen V., Yu J., Tirunagari S. et al. Large-eddy simulation of highly underexpanded transient gas jets [J]. *Physics of Fluids*, 2013, 25(1): 016101.

[19] Schmitt M., Hu Rennan, Wright Y. M. et al. Multiple cycle LES simulation of a direct injection natural gas engine [J]. *Flow Turbulence and Combustion*, 2015, 95(4): 645-668.

[20] Ghaseml A., Pereira A., Li X. Large eddy simulation of compressible subsonic turbulent jet starting from a smooth contraction nozzle [J]. *Flow Turbulence and Combustion*, 2017, 98: 83-108.

[21] Peng G., Yang C., Oguma Y. et al. Numerical analysis of cavitation cloud shedding in a submerged water jet [J]. *Journal of Hydrodynamics*, 2016, 28(6): 986-993.